LETTER

# Highly efficient computer algorithm for identifying layer thickness of atomically thin 2D materials

Letters

IOP Publishing

Journal of Physics D: Applied Physics

J. Phys. D: Appl. Phys. **51** (2018) 11LT03 (7pp)

https://doi.org/10.1088/1361-6463/aaac19

Letter

# Highly efficient computer algorithm for identifying layer thickness of atomically thin 2D materials

**Jekwan Lee[1,7], Seungwan Cho[1,7], Soohyun Park[1], Hyemin Bae[1], Minji Noh[1], Beom Kim[1], Chihun In[1], Seunghoon Yang[2], Sooun Lee[3], Seung Young Seo[4], Jehyun Kim[5], Chul-Ho Lee[2], Woo-Young Shim[3], Moon-Ho Jo[4,6], Dohun Kim[5] and Hyunyong Choi[1]**

[1] School of Electrical and Electronic Engineering, Yonsei University, Seoul 120-749, Republic of Korea
[2] KU-KIST Graduate School of Converging Science and Technology, Korea University, Seoul 02841, Republic of Korea
[3] Department of Materials Science and Engineering, Yonsei University, Seoul 120-749, Republic of Korea
[4] Department of Materials Science and Engineering, Pohang University of Science and Technology (POSTECH), Pohang 37673, Republic of Korea
[5] Department of Physics and Astronomy, Seoul National University, Seoul 08826, Republic of Korea
[6] Center for Artificial Low Dimensional Electronic Systems, Institute for Basic Science (IBS), Pohang 37673, Republic of Korea

E-mail: hychoi@yonsei.ac.kr

Received 18 December 2017, revised 22 January 2018
Accepted for publication 31 January 2018
Published 22 February 2018

**Abstract**

The fields of layered material research, such as transition-metal dichalcogenides (TMDs), have demonstrated that the optical, electrical and mechanical properties strongly depend on the layer number *N*. Thus, efficient and accurate determination of *N* is the most crucial step before the associated device fabrication. An existing experimental technique using an optical microscope is the most widely used one to identify *N*. However, a critical drawback of this approach is that it relies on extensive laboratory experiences to estimate *N*; it requires a very time-consuming image-searching task assisted by human eyes and secondary measurements such as atomic force microscopy and Raman spectroscopy, which are necessary to ensure *N*. In this work, we introduce a computer algorithm based on the image analysis of a quantized optical contrast. We show that our algorithm can apply to a wide variety of layered materials, including graphene, $MoS_2$, and $WS_2$ regardless of substrates. The algorithm largely consists of two parts. First, it sets up an appropriate boundary between target flakes and substrate. Second, to compute *N*, it automatically calculates the optical contrast using an adaptive RGB estimation process between each target, which results in a matrix with different integer *N*s and returns a matrix map of *N*s onto the target flake position. Using a conventional desktop computational power, the time taken to display the final *N* matrix was 1.8 s on average for the image size of 1280 pixels by 960 pixels and obtained a high accuracy of 90% (six estimation errors among 62 samples) when compared to the other methods. To show the effectiveness of our algorithm, we also apply it to TMD flakes transferred on optically transparent *c*-axis sapphire substrates and obtain a similar result of the accuracy of 94% (two estimation errors among 34 samples).

[7] Co-first authors.

 

Keywords: 2D material, layer thickness, layer number, contrast spectroscopy

(Some figures may appear in colour only in the online journal)

The first successful isolation of graphene in 2004 was done by mechanical exfoliation, so called the 'scotch tape' method. Since then, this method enabled us to open new research areas of two-dimensional (2D) atomic crystals and later expanded to the gapped 2D materials such as transition metal dichalcogenides (TMDs) [1–9]. Strong in-plane covalent bonding makes these materials form 2D crystal structures and weak out-of-plane van der Waals bonding allows us to isolate down to a monolayer (ML) limits in a relatively easy way [10–18]. The unique electrical, optical, and mechanical properties of 2D materials become evident as the number of layer $N$ approaches 1, where the reduced dielectric constant and enhanced Coulomb interaction are significantly enlarged compared to the bulk counterparts [8, 9, 19–23]. Because the characteristics of 2D materials emerge when $N$ is close to 1, a number of thin film synthesis methods have been proposed and demonstrated, and showed intriguing potentials for large-scale device applications; yet these techniques require sophisticated experimental facilities and well-controlled growth parameters to minimize polymorphic thin-film synthesis [24–30].

Although the advantages of mechanical exfoliation are clear in terms of single-crystal-like quality, accurate determination with a high successful rate for identifying exact $N$ relies on an empirical knowledge. In the 'scotch tape' method, the mechanically exfoliated flakes are transferred onto a suitable substrate first. Then, the sample is positioned under an optical microscope and scanned with a help of a translational stage. By moving the field of view of the sample continuously, one hopes to find an appropriate color contrast between the target flake and substrate. It is this step that takes most of time in identifying $N$. Even if an appropriate flake is selected, one needs secondary measurements, such as atomic force microscopy (AFM) and Raman spectroscopy to ensure $N$. Thus, the mechanical exfoliation method is not a simple process, but indeed a very time-consuming task requiring additional measurements for confirmation, which overall takes approximately a few hours. Prior investigations to identify N include optical image analysis taken from the optical microscopy; there, various numerical methods based on electromagnetic simulations were proposed to analyze the observed optical contrast distribution [31–36]. Motivated by the earlier works, our approach is to develop a very simple, and yet efficient, computer algorithm with minimal laboratory hardwares. For that reason, several researches have done to identify $N$ only with the optical microscopy based on the theoretical study of the observed optical contrast distribution [31–36]. Getting inspired by those methods, we approached this subject with the applicative point of view.

Here, we report a computer algorithm that automatically identifies $N$ down to 1 with less than 2 s. Our proposed method is similar to the 'scotch tape' method in a sense that it compares the optical contrast between flakes and substrate, but greatly reduces the flake-searching time to a second level with a very high accuracy (>90%) regardless of the substrates used. The software used in this work is based on the commercially available one, such that any research laboratory can incorporate easily the algorithm into existing analysis tools. We also used conventional laboratory hardwares, including optical microscope, CCD camera, and illumination light sources, so that the variation of computation errors when implemented in different laboratory should be zero.

Figures 1(a) and (b) show the schematics of the measurement setup and the corresponding overview of our algorithm, respectively. Mechanically exfoliated flakes are transferred on either a $Si/SiO_2$ wafer or a sapphire wafer. The image of appropriate samples is taken using a conventional optical microscope and CCD camera. This image becomes an input into a computer program and is analyzed through two major steps: boundary detection and layer estimation. After all of these processes, the computer produces an image of the estimated $N$.

Figure 1(b) represents the overall flow of our algorithm for $N$ determination. The schematics show (i) flake and image preparation and (ii) the main algorithm of boundary detection and layer estimation. For the flake preparation, we used prototypical 2D layered materials of graphene, $MoS_2$, and $WS_2$ using a mechanical exfoliation technique with 3 M Scotch tape™ and PDMS (X4 17.0 mil, Gel-Pak®). A silicon wafer with 300 nm thick $SiO_2$ layer or $c$-axis sapphire wafer was used as a substrate. Optical images were obtained by a CCD camera (UCMOS05100KPA, Hangzhou ToupTek Photonics Co., Ltd) attached to a conventional optical microscope (XY-MR microscope, Ningbo Sunny Instruments Co., Ltd) with two objective lenses (MPLFLN50× and MPLFLN100×, Olympus Co.) with LED light illumination. The sample was scanned by a motorized stage and a stage controller (EKSMA optics) before taking the optical image. The size of one image is 1280 pixels by 960 pixels, which covers the optical field of view of about 195 $\mu$m by 260 $\mu$m when ×50 objective is used. The MATLAB program was used for implementing the algorithm and a conventional desktop computer with Intel® Core™ i7-2660K CPU, Intel® HD Graphics 3000 graphic card, and 8.00 GB RAM is used. To verify the thickness of samples, AFM (XE-100, Park Systems) and an Raman spectrometer (Lab Ram ARAMIS, Horiba Ltd.) were used.

The mechanically exfoliated flakes enter into the image preparation step. Figure 2(a) is an example of the processed results of the boundary detection using graphene, where the top and bottom images are the optical microscope and the processed image after the boundary detection. The algorithm takes the optical images of an empty wafer and a few layer flakes, and the images are converted into a luminescence $[m \times n]$ $\boldsymbol{I}$ matrix. Here, $m$ and $n$ is the size of row and column of the image pixel number, and the matrix elements of luminescence are RGB values. With $\boldsymbol{I}$, the boundary between regions of different $N$ is defined by calculating a relative variance matrix $\boldsymbol{V}$ which can be derived by convolving $\boldsymbol{I}$ with the scanning window matrix $\boldsymbol{W}$. The scanning window matrix is a square matrix filled with a

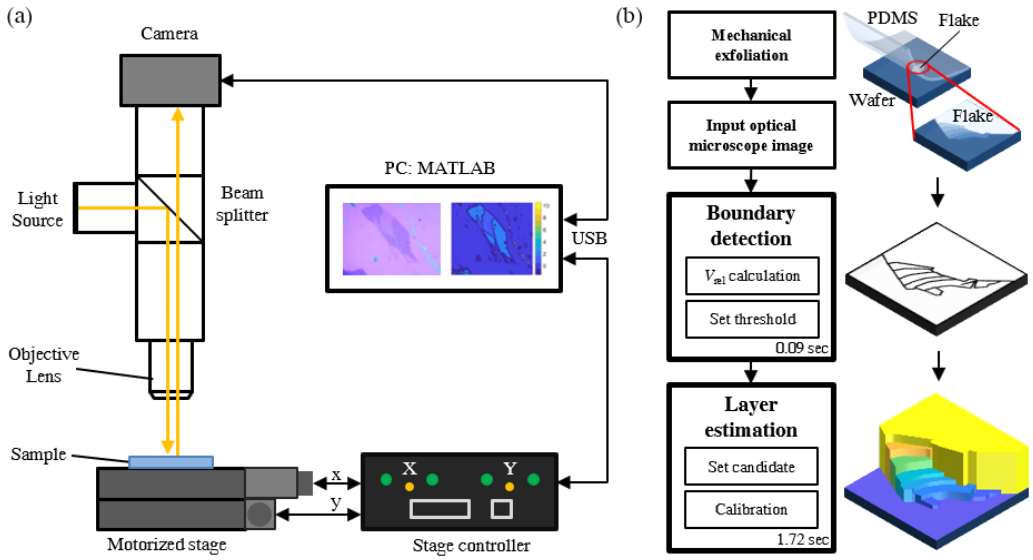


**Figure 1.** (a) Schematic diagrams of the *N* estimation setup. All components are based on conventional laboratory hardwares, softwares and desktop computational powers. See text for more detailed specifications. (b) Schematic illustration of the *N*-estimation algorithm. Image analysis of the mechanically exfoliated samples largely consists of two main steps: boundary detection and layer estimation, in which the former takes about 0.09 s and the latter about 1.72 s.

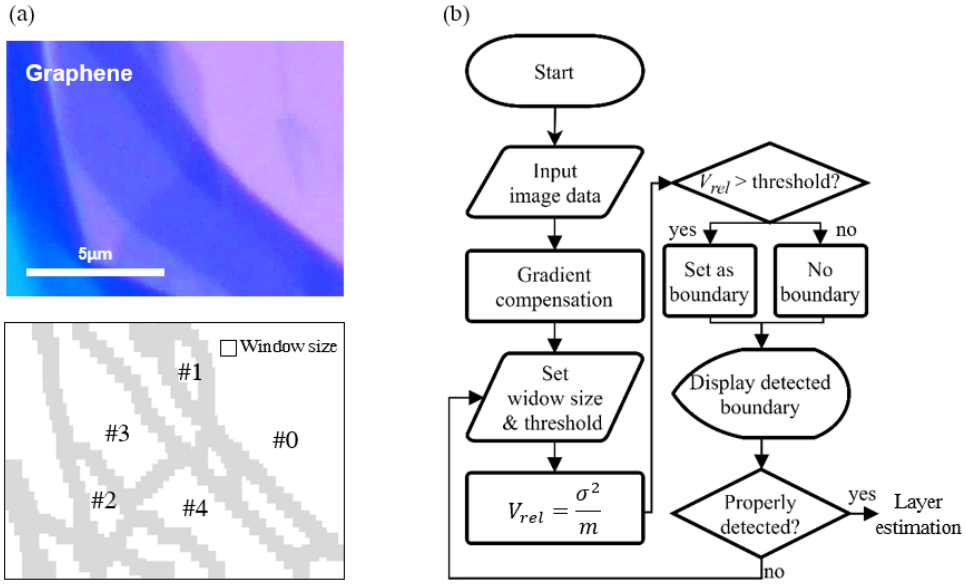


**Figure 2.** (a) Optical microscopy image (top) and boundary detected image (bottom) of exfoliated graphene. The window size is exaggerated for clarity. Scale bar in the upper image is 5 $\mu$m. The divided region in the lower image is numbered for arrangement. (b) A flowchart of the boundary detection algorithm. By calculating the relative variance inside the window and set proper threshold to decide boundary, windows locating at the boundary of the region are filled with null value which represented as gray color.

fixed value (1/window size$^2$). By taking convolution between $\boldsymbol{I}$ and $\boldsymbol{W}$, the mean variable matrix $\boldsymbol{M}$ is calculated. Mathematical equivalence of the above procedure is expressed as,

$$\boldsymbol{M} = \boldsymbol{I}^{*}\boldsymbol{W}, \boldsymbol{M}' = \boldsymbol{I}'^{*}\boldsymbol{W}, \quad I'_{ij} = I_{ij}^2, \\ (i = 1, \cdots, m, j = 1, \cdots, n). \tag{1}$$

We also calculate another mean variable matrix $\boldsymbol{M}'$ of the squared luminance matrix $\boldsymbol{I}'$ to derive the relative variance as written in equation (1).

$$V_{ij} = \frac{M'_{ij} - M_{ij}^2}{M_{ij}}. \tag{2}$$

Equation (2) shows the derivation of the variance matrix $\boldsymbol{V}$ by subtracting each matrix element of $\boldsymbol{M}$ from $\boldsymbol{M}'$, which is then normalized by the matrix component of $\boldsymbol{M}$. Using this variance distribution information, the boundary is marked by filling the window with a null value if the relative variance of the pixels in the window is beyond a user-defined threshold. There, the regions with different *N* are separated into pieces for further layer counting process. In figure 2(a), the boundary is colored with a gray color based on the given window size and the separated regions, which are labeled with different numbers (note the size of the window is exaggerated in the figure). The flow chart of this step is shown in figure 2(b). The feedback loop is

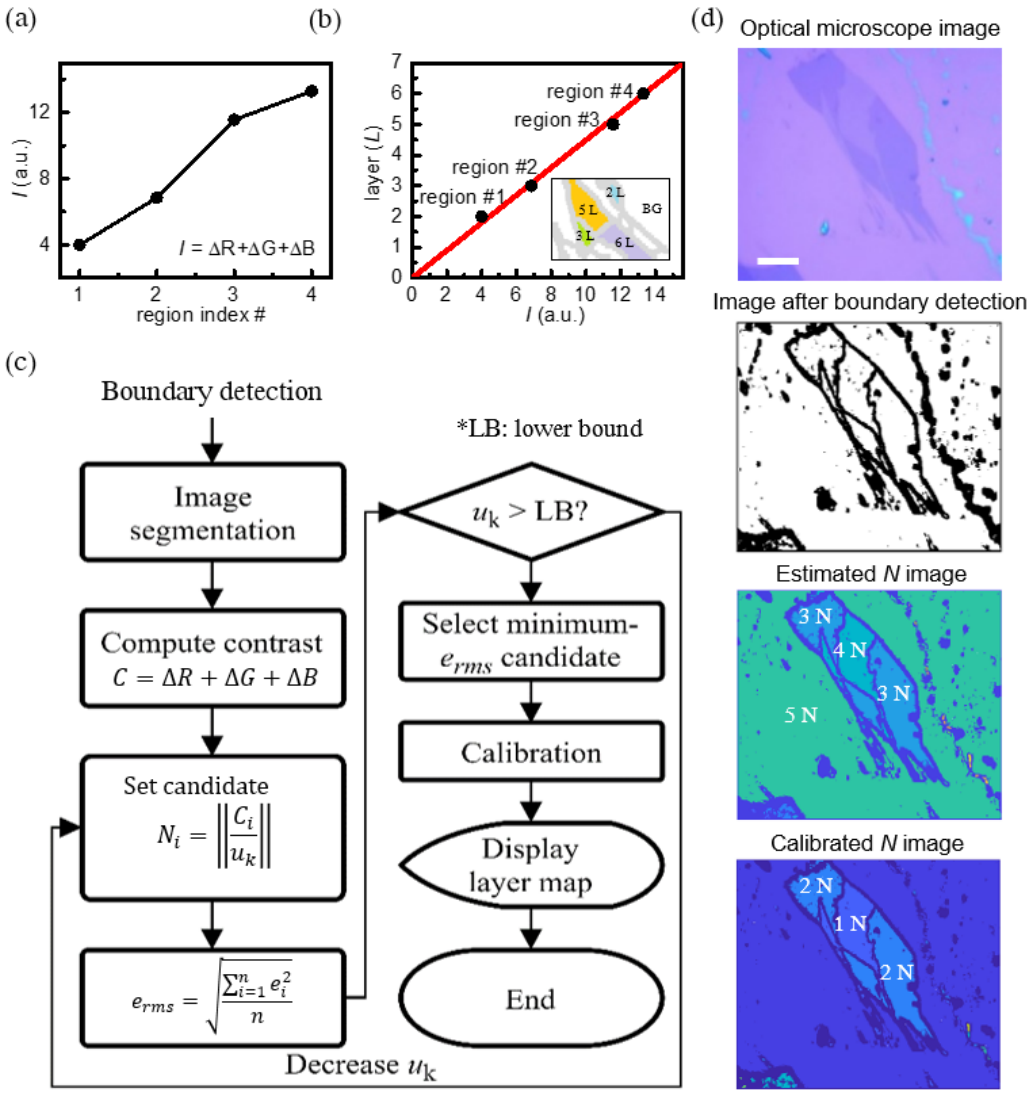


**Figure 3.** (a) Calculated matrix element of $I$ is shown for each region index. Here, figure 2(a) is used as an example. (b) The estimated $N$ is plotted as a function of $I$. Red line represents a linear relationship between $N$ and $I$. Black dots are the indexed regions in figure 2(a). Inset shows the image representation of the result. (c) A flowchart of the layer estimation algorithm. Based on boundary detection result, image is divided into boundary-surrounded regions and layer is estimated by contrast and RMS error calculation. Finally, estimated result is calibrated to eliminate the effect of substrate reflection. (d) Examples of graphene are shown after processing each algorithm step.

necessary to increase the accuracy, where the size of the window and threshold value are the control parameters.

The second main step after boundary detection is the $N$ estimation process. Previous studies [31, 33–36] have shown that the optical contrast linearly increases with layer thickness as long as the thickness is less than 10 nm. The optical contrast of a few-layer materials can be quantized by the contrast of single layer, and therefore $N$ can be estimated accordingly. With the boundary data from the first step, the algorithm calculates the average value of the matrix element of $\boldsymbol{I}$ of each region and rearrange $\boldsymbol{I}$ using the updated averages. An example after this sorting process is plotted in figure 3(a). To calculate the contrast of each region, we use the following formula [34]:

$$C = \frac{I_{\text{flake}} - I_{\text{substrate}}}{I_{\text{flake}} + I_{\text{substrate}}},$$

$$\boldsymbol{C} = \{C_1, C_2, \cdots, C_n\},$$

where $\boldsymbol{C}$ is a set of contrast values. We assume the smallest luminance region is the substrate one in this process. Obviously, since the unit contrast $u$ should be the same or smaller than the minimum contrast difference measured in the sample image, we design the algorithm to start from the minimum value of the detected contrast difference:

$$\text{Lower bound} < u \leqslant \min(C).$$

The program then sweeps down $u$ from the minimum value detected from image contrast difference continuously to user-defined lower bound and calculates the root-mean-square (RMS) error for each candidate. The lower bound of $u$ is set as an user-defined value. This is simply because different laboratory has different experiment conditions. Nevertheless, the suitable lower bound can be found via dividing the minimum contrast difference by an expected $N$ of the region exhibiting a least contrast difference, and then the program optimizes $u$ by running a feedback algorithm.

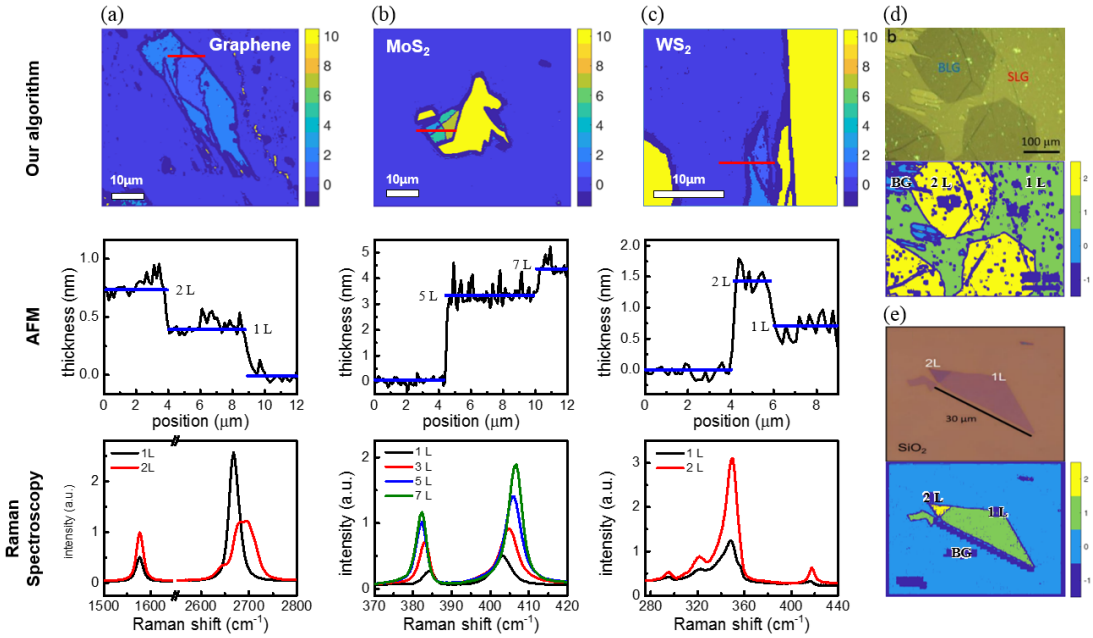


**Figure 4.** We compare our algorithm results of $N$ determination to other methods of AFM and Raman, and even compared to the published results. The AFM and Raman comparison for graphene, $MoS_2$, and $WS_2$ is shown in (a)–(c), respectively. Scale bar is 10 $\mu$m. The color bar notates color usage for displaying $N$ in our result. Boundary is marked by $N = -1$. (d) Top: a graphene image reprinted from Carbon 107, Chen *et al* 'Chemical vapor deposition growth of large single-crystal bernal-stacked bilayer graphene from ethanol', 852–6. Reprinted from [40], Copyright 2016, with permission from Elsevier. Bottom: the result of our algorithm. (e) Top: a $MoS_2$ image from Castellanos-Gomez *et al* 2014 Mechanics of freely-suspended ultrathin layered materials. [41] John Wiley & Sons. © 2014 by WILEY-VCH Verlag GmbH & Co. KGaA, Weinheim. Bottom: the result of our algorithm.

To compare the estimation result with the measured contrast, individual estimation error $e_i$ is computed by subtracting the natural number $j$ multiplication of $u$ from the closest measured contrast, which we define it as a minimum value of difference among all possible $u \cdot j$ combinations. The RMS error is, then, calculated with $e_i$:

$$e_i = \min(C_i - u \cdot j)(j = 1, 2, 3, \cdots) \tag{3}$$

$$e_{\text{rms}} = \sqrt{\frac{\sum_{i=1}^{n} e_i^2}{n}}. \tag{4}$$

After calculating the RMS error $e_{\text{rms}}$, the program returns the contrast value of each image region. Because a candidate with the smallest $e_{\text{rms}}$ is expected to be the desired unit contrast, we use $e_{\text{rms}}$ as an indicator to choose the most possible candidate. Finally, the estimated layer number $N$ of each region is calculated by dividing $C$ with $u$ and round it:

$$N_i = \left\| \frac{C_i}{u} \right\| \quad (i = 1, 2, \cdots, n). \tag{5}$$

Figure 3(b) shows the estimation result. Once the $u$ is determined, $N$ is obtained for each region by the linear relationship between $C$ and $N$. A flow chart shown in figure 3(c) summarizes the $N$ estimation process after the boundary detection. We note that there is only one parameter—a lower bound for the unit contrast candidate—for our $N$ estimation algorithm.

The contrast values are different depending on the substrates used, because the reflection coefficient varies. This consideration is also included in our algorithm as a calibration process. For example, when an optically transparent substrate such as sapphire is used, we consider the reflection from the flakes only, from which the contrast simply increases as the flakes become thicker. On the other hand, for a reflective substrate such as Si/$SiO_2$ and copper, the substrate appears to be brighter than the flakes because of the multiple reflection from the substrate, causing negative contrast values. This problem can be resolved by manually selecting the substrate region and checking out if there is any region that exhibits a weak luminance than the substrate. When such a region is detected, the algorithm calls for the contrast values and computes again on the basis of the selected substrate region. Figure 3(d) shows an example of such calibration process when the Si/$SiO_2$ substrate was used. As shown in the third row, $N$ was estimated to be 5 before calibration. By selecting a different substrate region, the difference of $N$ between the substrate and the flakes is set as a new $N$. The calibrated result is presented in the last row of figure 3(d).

To show that our algorithm is applicable to other layered 2D materials, we compared our algorithm results with the conventional $N$-confirmation methods of AFM and Raman spectroscopy. The comparison is shown in figures 4(a)–(c), where the images are the mechanically exfoliated graphene, $MoS_2$, and $WS_2$ flakes transferred onto a standard Si/$SiO_2$ substrate. After testing 62 flakes on a Si/$SiO_2$ substrate and 34 flakes on a transparent sapphire substrate, we have achieved the accuracy of 90% for Si/$SiO_2$ substrate and 94% for the sapphire substrate.

Our algorithm shows several advantages over the AFM and Raman measurements. For the AFM method, when a thin flake is located right next to a thick flake and is far apart from the substrate, the thickness of the thinner part is measured as if it has

a similar thickness to the thicker part. In addition, there always exists nontrivial spikes between each flake fraction with different thickness when performing the partial line-cut measurement. This oscillatory profile sometimes makes one confused in distinguishing the different thickness. Despite the Raman spectroscopy does not have such issues, it has low versatility on determining $N$ when applied into different types of layered 2D materials. We found that although the Raman spectroscopy is able to confirm $N$ for graphene and $MoS_2$ relatively in a straightforward way due to the large Raman shift [37, 38], the Raman signal of $WS_2$ does not exhibit such a large shift [39]. Typically, one resolves this issue by performing multiple measurements and crosschecking the results with other secondary methods, such as transmission electron microscopy (TEM), which requires an extra amount of laboratory times. Another advantage of our algorithm is that it can identity $N$ regardless of different experiment conditions. Figures 4(d) and (e) show the images taken from published literatures [40, 41]. Although the laboratory conditions, such as light illumination, magnification of lens, substrates, and sample preparation methods, are different, our algorithm identifies exactly the same $N$ for the above images. The computation time is also an important aspect in our algorithm. Under the given computational powers (Intel® Core™ i7-2660K CPU, Intel® HD Graphics 3000 graphic card, and 8.00 GB RAM), our algorithm takes ~1.8 s for the image size of 1280 pixels by 960 pixels (195 $\mu$m by 260 $\mu$m with $\times$50 objective lens). This implies that our method can be implemented into a thin-film growth facility, enabling *in situ* inspection of $N$, before finishing the growth process.

In summary, we proposed a highly efficient computer algorithm to determine $N$ of layered 2D materials. The algorithm largely consists of a boundary detection and $N$ estimation process. The accuracy was compared to the results of conventional AFM and Raman measurements. In addition, our algorithm can be applied into various 2D layered materials even if the experimental conditions are different. We expect that our proposed method can significantly reduce the $N$-searching laboratory time, and furthermore it is very cost effective compared to any other methods for the $N$ determination.

## Acknowledgments

JL, SC, SP, HB, MN, BK, CI and HC were supported by the National Research Foundation of Korea (NRF) through the government of Korea (MSIP) (Grant Nos. NRF-2015R1A2A1A10052520, NRF-2016R1A4A1012929, NRF-2017M3D1A1040828), Global Frontier Program (2014M3A6B3063709). S-YS and M-HJ were supported by the Institute for Basic Science (IBS), Korea, under project code IBS-R014-A1. C-HL acknowledges the support from National Research Foundation (NRF) of Korea (2017R1D1A1B03035441) and the KU-KIST School Project. DK was supported by the Basic Science Research Program through the NRF funded by the Ministry of Science, ICT and Future Planning (Grant No. NRF-2015R1C1A1A02037430).

## ORCID iDs

Jekwan Lee https://orcid.org/0000-0001-7817-1123

## References

[1] Novoselov K S, Geim A K, Morozov S V, Jiang D, Zhang Y, Dubonos S V, Grigorieva I V and Firsov A A 2004 *Science* **306** 666–9
[2] Geim A K and Novoselov K S 2007 *Nat. Mater.* **6** 183–91
[3] Geim A K 2009 *Science* **324** 1530–4
[4] Novoselov K S, Fal'ko V I, Colombo L, Gellert P R, Schwab M G and Kim K 2012 *Nature* **490** 192–200
[5] Novoselov K S, Jiang D, Schedin F, Booth T J, Khotkevich V V, Morozov S V and Geim A K 2005 *Proc. Natl Acad. Sci. USA* **102** 10451–3
[6] Wilson J A and Yoffe A D 1969 *Adv. Phys.* **18** 193–335
[7] Ayari A, Cobas E, Ogundadegbe O and Fuhrer M S 2007 *J. Appl. Phys.* **101** 014507
[8] Wang Q H, Kalantar-Zadeh K, Kis A, Coleman J N and Strano M S 2012 *Nat. Nanotechnol.* **7** 699–712
[9] Jariwala D, Sangwan V K, Lauhon L J, Marks T J and Hersam M C 2014 *ACS Nano* **8** 1102–20
[10] Coleman J N 2009 *Adv. Funct. Mater.* **19** 3680–95
[11] Coleman J N 2013 *Acc. Chem. Res.* **46** 14–22
[12] Cui X, Zhang C, Hao R and Hou Y 2011 *Nanoscale* **3** 2118–26
[13] Dreyer D R, Park S, Bielawski C W and Ruoff R S 2010 *Chem. Soc. Rev.* **39** 228–40
[14] Loh K P, Bao Q, Ang P K and Yang J 2010 *J. Mater. Chem.* **20** 2277–89
[15] Cai M, Thorpe D, Adamson D H and Schniepp H C 2012 *J. Mater. Chem.* **22** 24992
[16] Yi M and Shen Z 2015 *J. Mater. Chem.* A **3** 11700
[17] Hernandez Y *et al* 2008 *Nat. Nanotechnol.* **3** 563–8
[18] Paton K R *et al* 2014 *Nat. Mater.* **13** 624–30
[19] Novoselov K S, Geim A K, Morozov S V, Jiang D, Katsnelson M I, Grigorieva I V, Dubonos S V and Firsov A A 2005 *Nature* **438** 197–200
[20] Horng J *et al* 2011 *Phys. Rev.* B **83** 165113
[21] Zhang Y, Tang T-T, Girit C, Hao Z, Martin M C, Zettl A, Crommie M F, Ron Shen Y and Wang F 2009 *Nature* **459** 820–3
[22] Ulstrup S *et al* 2014 *Phys. Rev. Lett.* **112** 257401
[23] Mattheis L F 1973 *Phys. Rev.* B **8** 3719–40
[24] Li X *et al* 2009 *Science* **324** 5932
[25] Kim K S, Zhao Y, Jang H, Lee S Y, Kim J M, Kim K S, Ahn J-H, Kim P, Choi J-Y and Hong B H 2009 *Nature* **457** 706–10
[26] Li X, Cai W, Colombo L and Ruoff R S 2009 *Nano Lett.* **9** 4268–72
[27] Chhowalla M, Shin H S, Eda G, Li L-J, Loh K P and Zhang H 2013 *Nat. Chem.* **5** 263–75
[28] Liu K *et al* 2012 *Nano Lett.* **12** 1538–44
[29] Shi Y *et al* 2012 *Nano Lett.* **12** 2784–91
[30] Zhan Y, Liu Z, Najmaei S, Ajayan P M and Low J 2012 *Small* **8** 966–71
[31] Li Y, Dong N, Zhang S, Wang K, Zhang L and Wang J 2016 *Nanoscale* **8** 1210–5
[32] Li H, Wu J, Huang X, Lu G, Yang J, Lu X, Xiong Q and Zhang H 2013 *ACS Nano* **7** 10344–53
[33] Gao L, Ren W, Li F and Cheng H-M 2008 *ACS Nano* **2** 1625–33
[34] Castellanos-Gomez A, Agraït N and Rubio-Bollinger G 2010 *Appl. Phys. Lett.* **96** 213116

[35] Wang Y Y, Gao R X, Ni Z H, He H, Guo S P, Yang H P, Cong C X and Yu T 2012 *Nanotechnology* **23** 495713
[36] Blake P, Hill E W, Castro Neto A H, Novoselov K S, Jiang D, Yang R, Booth T J and Geim A K 2007 *Appl. Phys. Lett.* **91** 063124
[37] Hao Y, Wang Y, Wang L, Ni Z, Wang Z, Wang R, Koo C K, Shen Z and Thong J T L 2009 *Small* **6** 195–200
[38] Boukhicha M, Calandra M, Measson M-A, Lancry O and Shukla A 2013 *Phys. Rev.* B **87** 195316
[39] Berkdemir A *et al* 2013 *Sci. Rep.* **3** 1755
[40] Chen X, Xiang R, Zhao P, Inoue H A T, Chiashi S and Maruyama S 2016 *Carbon* **107** 852–6
[41] Castellanos-Gomez A, Singh V, van der Zant H S J and Steele G A 2014 *Ann. Phys.* **527** 27–44